J. Indian Inst. Sci., 66, Apr. 1986, pp. 263–292

IISc THESES ABSTRACTS

Thesis Abstract (Ph.D.)

Vibrational spectroscopic and dielectric studies of some ferroic crystals by B. Raghunatha Chary.
Research supervisors: P. S. Narayanan and H. L. Bhat.
Department: Physics

1. Introduction

Alkali metal double sulphates belong to the family of compounds represented by the general formula $M'M''Bx_4$. The crystals belonging to this family are very interesting in the sense that they have different phase transition schemes and show wide variety of physical properties. For example, $LiNH_4SO_4$ is ferroelectric in the range 10° to 180°C[1]. $LiKSO_4$ has also been established to have a ferroelectric phase[2]. On the other hand, $LiCsSO_4$ is known to undergo a second order ferroelastic phase transition at 202°K accompanied by softening of an acoustic mode[3]. $LiRbSO_4$, though belonging to the same family, shows entirely different phase transition schemes with a sequence of four structural phase transitions above room temperature, the phase between 202° and 204°C being reported as incommensurate[4].

Another set of crystals which are equally interesting are those belonging to the langbeinite family represented by the general formula $A_2^+B_2^{2+}(SO_4)_3$. Many crystals belonging to this family also undergo phase transitions and some of them show ferroelectric and ferroelastic phases[5]. The main interest in this family of crystals is because the true order parameter does not seem to be the spontaneous polarization.

In this thesis some of the crystals belonging to the above two families are investigated through vibrational spectroscopic and dielectric studies with an objective to gain insight into the nature of phase transition and to understand the role of SO_4 group in the transition. The crystals investigated are $LiCsSO_4$ (LCS), $LiRbSO_4$ (LRS), $K_2Mn_2(SO_4)_3$ (KMS), $(NN_4)_2Mn_2(SO_4)_3$ (AMS), and $K_2Zn_2(SO_4)_3$ (KZS). The results were also supplemented by DSC data.

2. Experimental work

LCS, LRS, KMS and AMS were grown by aqueous solution method while KZS was grown by melt technique. For the former, an indigeneously-built crystal growth apparatus was used, wherein crystals could be grown either by solvent evaporation or temperature lowering. All the Raman spectra were recorded using a SPEX RAMALOG-6 double monochromator spectrometer. A Spectra-Physics 165 model Argon ion laser operating at 4880 Å line was used as exciting line. The IR spectra

were recorded using a Perkin-Elmer 580 model spectrometer. A Specac variable temperature assembly was used to record the low temperature spectra. A home-made high temperature thermostatic system was used to record the spectra at high temperatures. The DSC traces were taken using a Perkin-Elmer DSC-2 differential scanning calorimeter with Indium as standard. For dielectric studies under high pressures a piston cylinder type high pressure cell which could go up to 8 Kbar was designed and fabricated[6].

3. Results and conclusions

The study of the temperature dependence of external modes in different polarisation settings of the LCS crystal precluded the presence of any soft optical phonon mode. Based on this, it can be said that phase transition in LCS is likely to be a true proper ferroelastic one, where the spontaneous strain developed in the ferroelastic phase, is the order parameter of the transition[7]. Our Raman spectroscopic study of both external and internal modes across the phase transition reveals that a continuous phase transition associated with gradual structural changes is taking place in LCS. The observed anomaly in the total integrated area of the totally symmetric ν_1 mode in (aa) and (ac) polarisations across the transition is attributed to increase of fluctuations in the polarisability of the scattering species. From the observed dielectric anomalies along the b-axis of LCS crystal in the heating run under various hydrostatic pressure it can be seen that transition temperature T_c shifts towards the lower side with the increase of pressure and the peak value of dielectric constant decreases. Change in T_c with pressure is linear up to 5 Kbars above which it deviates from linearity. The value of dT_c/dp is closer to the value obtained from using Ehrenfest relation[8]. The negative value for dT_c/dp is consistent with the reported volume thermal expansion coefficient of LCS which shows a negative anomaly at transition temperature.

The polarised Raman spectra of LRS at room temperature agree reasonably well with group theoretical predictions. A comparison of room temperature Raman spectra of LRS with LCS in its low temperature phase shows that the replacement of Cs with Rb atoms brings about an upward shift in lattice frequencies. But internal mode frequencies of sulphate ions in the C_{2h} phases of LRS and LCS do not differ significantly. The observed maxima in the total areas of ν_1, ν_2 and ν_4 modes in the vicinity of incommensurate phases are attributed to the fluctuations in polarisability of SO_4^{2-} ions reaching a large value in this temperature region[9]. The IR absorption spectrum at room temperature showed the expected (A_u+B_u) symmetry species.

Raman spectra of KMS recorded in the internal mode region in the cubic and orthorhombic phases differ significantly and this could be associated with change in symmetry across transition. Based on IR and Raman spectra, it was concluded that phase transition in KMS was connected with reorientation of SO_4 groups resulting in the low temperature ordered phase. For AMS, the appearance of extra lines in the F species Raman spectrum in the SO_4 internal mode region was interpreted as due

to LO-TO splitting[10]. The large bandwidth and frequency shift observed in NH_4 group internal modes in Raman and IR spectra suggest the existence of N-H . . . . . O type hydrogen bonds in AMS. The vibrational spectra of KZS resemble closely with those of KMS and AMS.

Acknowledgement

The financial assistance of the Department of Science and Technology through a project grant is grately appreciated.

References

1. Mitsui, T., Oka, T., Shiroishi, Y., Takashige, M., Ito, K. and Sawada, S. — Ferroelectricity in NH_4LiSO_4, *J. Phys. Soc. Jap.*, 1975, **39**, 845–846.

2. Fujimoto, S., Yasuda, N., Hirino, H. and Narayanan, P. S. — Ferroelectricity in lithium potassium sulphate, *J. Phys. D*, 1984, **17**, L-35–37.

3. Aleksandrov, K. S., Zamseva, M. P. Shabanova, L. A. and Shimanskaya, O. V. — The elastic properties of ferroelectric $LiCsSO_4$ in the proximity of the phase transition, *Sov. Phys. Solid St.*, 1981, **23**, 1426–1428.

4. Mashiyama, H., Hasebe, K., Tanisaki, S., Shiroishi, Y. and Sawada, S. — X-ray studies on successive structural transitions in $RbLiSO_4$, *J. Phys. Soc.Jap.* 1979, **47**, 1198–1204.

5. Hikita, T., Kitabatake, M. and Ikeda, T. — Effect of hydrostatic pressure on the phase transitions of langbeinite-type crystals, *J. Phys. Soc. Jap.*, 1980, **49**, 1421–1428.

6. Raghunatha Chary, B., Bhat, H. L. and Narayanan, P. S. — Dielectric properties of ferroelastic $LiCsSO_4$ crystal under high pressure, *Proc. 3rd Natn. Seminar on ferroelectrics and dielectrics*, 1984, 374–381.

7. Wadhavan. V. K. — Ferroelasticity and related properties of crystals. *Phase Transitions*, 1982, **3**, 3–103.

8. Aleksandrov, K. S., Zherebtsova, L. I., Iskornev, I. M., Kruglik, A. I., Rozanov, O. V. and Flerov, I. N. — Investigation of structural and physical properties of cesium-lithium double sulfate, *Sov. Phys. Solid. St*, 1980, **22**, 2150–2152.

9. Raghunatha Chary, B., Bhat, H. L., Chandrasekhar, P. and Narayanan, P. S. — Vibrational spectroscopic studies of the ferroelectric $LiRbSO_4$, *J. Raman Spectro. sco.*, 1986, **17**, 59–63.

10. RAGHUNATHA CHARY, B., BHAT, H. L., CHANDRASEKHAR, P. AND NARAYANAN, P. S. Vibrational spectroscopic and thermal studies of phase transition in langbeinite type $K_2Mn_2(SO_4)_3$, *Proc. 3rd Natn. Seminar ferroelectrics dielectrics*, 1984, 315–322.

Thesis Abstract (Ph.D.)

Studies on the crystal growth and dielectric properties of alkali metal perchlorates by T. Shripathi.
Research supervisors: H.L. Bhat and P.S. Narayanan.
Department: Physics.

1. Introduction

The perchlorates of potassium, rubidium and cesium undergo structural phase transitions at elevated temperatures[1,2]. All the three perchlorates have an orthorhombic (Pnma) structure at room temperature. They undergo structural phase transitions at temperatures 301.5, 284.5 and 228°C respectively for $KClO_4$, $RbClO_4$ and $CsClO_4$ to cubic F4 3m or Fm 3m. The phase transition from orthorhombic to cubic has been studied earlier by X-ray, DTA, spectroscopic and dielectric measurements[3–6]. However, physical data on single crystal samples are scarce. This is probably due to their very low solubility in water at room temperature and they decompose on melting. It was therefore considered worthwhile to grow these materials in the single crystal form and to investigate their dielectric properties with the object of understanding the role of ClO_4 groups in their structural phase transition. This thesis reports the results obtained therein.

2. Experimental programme

Single crystals of $KClO_4$, $RbClO_4$ and $CsClO_4$ of several mm in length were grown. Silica gel technique was employed to grow these crystals for the reasons stated earlier. Optimum growth conditions were tried and final characterization was carried out. Growth kinetics, and effect of gel aging, concentration programming, pH variation, etc., on growth process have been studied.

Dielectric constants and loss were measured using an LCR bridge at 1 KHz to detect the phase transition. Dielectric behaviour of irradiated samples of $KClO_4$ was also investigated to study the effect of irradiation. A detailed dielectric analysis was then carried out over a frequency range of 1–30 KHz along the three crystallographic axes by coupling the bridge with an external oscillator and a lock-in-amplifier. Finally DC conductivity measurements were carried out on these crystals and their temperature variations studied.

3. Results and Conclusions

Growing crystals with low solubility is a very troublesome task. Using the gel technique and carrying out detailed growth studies these difficulties were overcome

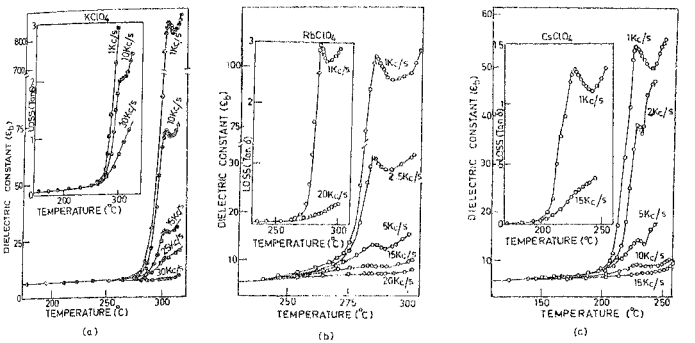

FIG. 1. Dielectric dispersion in a) $KClO_4$, b) $RbClO_4$, and c) $CsClO_4$.

and very clear single crystals of appreciable dimensions were grown (Some crystals had linear dimensions up to 10 mm). By careful experimentation growth conditions were optimised and it was found that the most suitable concentration for good quality crystals was in the range 0.2 M to 0.3 M of cation feed solution. Detailed growth kinetic studies indicate that the growth rate is diffusion-controlled. Post-growth mass spectrometric analysis showed that the crystals grown had very low impurity levels. Measurement of dielectric constant and tan δ and of conductivity in these crystals at various temperatures reveals a sharp increase at about 250, 240 and 200°C and anomalous behaviour at the transition temperatures. The measurement on irradiated samples show increased ϵ and tan δ values. The anomalous dielectric behaviour near the phase transition has been discussed in terms of existing Pauling[7] and Frenkel[8] models and has been attributed to the orientational disorder of the ClO_4 ions in the high temperature phase.

The dielectric dispersion studies have given some interesting results. As the frequency of the measuring signal increased, the peak value of the dielectric constant at the transition temperature goes on decreasing and flattens out (fig. 1). This flattening frequencies are 30, 20 and 15 KHz respectively for $KClO_4$, $RbClO_4$ and $CsClO_4$. Since the dielectric anomaly flattens out at radio frequency itself, the structural transition is explained in terms of Frenkel's model of increased orientational disorder. These results agree with the theoretical calculations done earlier. The interesting feature observed in the case of perchlorates is that the activation energy (from DTA results) associated with the phase transition and the frequency at which ϵ *vs* T curves flatten, have the same ratios, *i.e.*, 6:4:3 for all the crystals. This is understandable as both these quantities in a way are indicative of the measure of disorder in the system.

The dielectric behaviour T_c has been analysed in terms of complex electric modulus instead of usual Cole–Cole plot because these crystals were highly lossy at higher temperatures. The electric Modulus $M^* = (\epsilon^*)^{-1} M' + jM''$. The plot of M' vs M'' in the complex plane for these perchlorates are found to be circular arcs. From these plots the relaxation times were calculated and values thus obtained are for $KClO_4 = 2.6\,\mu s$, $RbClO_4 = 10\,\mu s$, and $CsClO_4 = 15.9\,\mu s$. The temperature variation of dc conductivity for these perchlorates show broadly three regions. These correspond to *intrinsic region, cation movement* region and to the precipitation region with activation energies around 1.5 eV, 0.80 eV and 0.1 eV respectively.

In conclusion, single crystals of K, Rb and Cs perchlorates have been grown by the gel technique. Their dielectric behaviour at the phase transition can be explained in terms of orientational disorder that sets in at the phase transition. The advantages of the dielectric analysis in terms of complex dielectric modulus have been fully utilised to interpret the high frequency values of dielectric constant.

References

1. BREDIG, M. A. — High-temperature crystal chemistry of A_mBX_n compounds with particular reference to calcium orthosilicate, *J. Phys. Chem.*, 1945, **49**, 537–553.
2. RAO, C. N. R. AND PRAKASH, B. — Crystal structure transformations in inorganic sulphates, phosphates, perchlorates and chromates. NSRDS Report, National Bureau of Standards, 1974, **56**, 22.
3. MOLEPO, J. M. — Ph.D. Dissertation, Hannover, FRG, 1975.
4. SØRØMME, K. O. — The crystal structure of orientationally disordered, cubic high-temperature phases of univalent metal perchlorates, *Acta Chem. Scand.*, 1974, **28A**, 515–527.
5. PAI VERNEKER, V. R. AND RAJESHWAR, K. — Crystal structure transformation in ammonium and alkali metal perchlorates, *Thermochim. Acta*, 1975, **13**, 305–314.
6. SYAL, S. K. AND YOGANARASIMHAN, S. R. — Infrared and permittivity studies on alkali perchlorates, *J. Solid St. Chem.*, 1974, **10**, 332–340.
7. PAULING, L. — The rotational motion of molecules in crystals, *Phys. Rev.*, 1930, **36**, 430–443.
8. FRENKEL, J. — Über die Drehung Von dipolmolekülen in festen Körpern, *Acta Physicochim. U. R. S. S.*, 1935, **3**, 23–36.

Thesis Abstract (Ph.D.)

Strategies of synthesis based on methoxycyclohexadienes: Synthesis of some polyketides by N. S. Mani.
Research Supervisor: G. S. R. Subba Rao.
Department: Organic Chemistry.

1. Introduction

The polyketides[1] are a group of natural products consisting of anthraquinones,

alkyl resorcylates, flavonoids, isoflavonoids, xanthones and macrocyclic lactones, etc., and are biogenetically derived from a two-carbon unit, acetic acid. Some of these compounds are biologically active as antibiotics and hence total syntheses of these molecules will be of interest. Synthesis of these precursors will be of immense use in understanding the biosynthetic mechanisms involved in the formation of secondary metabolites. In view of this, a strategy has been developed[2] to synthesize the aromatic polyketides which involves the construction of the aromatic moiety by the cycloaddition of methoxycyclohexadienes with acetylenic dienophiles using the Alder–Rickert reaction. This new methodology differs from the conventional routes involving the elaboration of the appropriate aromatic compounds. By using this method, synthesis of mellein, lasiodiplodin, curvularin, stemphol and antibiotic DB-2073 have been achieved. A new route to mycophenolic acid has also been explored.

2. Results and discussion

1-Methoxycyclohexa-1,4-dienes (2) have been readily prepared[3] by the metal-ammonia reduction of anisoles (1). These dienes undergo isomerization to 1-methoxycyclohexa-1,3-dienes (3) in the presence of bases or under autocatalytic conditions with dienophiles. Reaction of 1-methoxycyclohexa (1,4) or (1,3)-dienes with methyltetrolate at 180° afforded an adduct (4) which on thermolysis yielded methyl 2-methoxy 6-methylbenzoate (5) quantitatively. Similarly reaction of 1,3-dimethoxycyclohexa-1,3-diene (6) with methyl tetrolate gave methyl 2,4-dimethoxy-6-methyl benzoate (7). Thus a simple and efficient method[2] for the synthesis of alkyl salicylates and alkyl resorcylates, the precursors of polyketides has been devised. In this reaction, the regiochemistry of addition has been established. This reaction has been extended to some important polyketides of biological interest.

Reaction of (2) or (3) with the acetylenic ester (8), prepared from propiolic ester, yielded the adduct (9a) which on pyrolysis followed by demethylation afforded mellein[4] (10a). Similarly, reaction of (6) with (8) yielded 6-methoxymellein[5] (10b) through the adduct (9b). Reaction of the diene (6) with the acetylenic dienophiles (11) and (12), prepared by standard methods, yielded lasiodiplodin[6] (13) and curvularin[7] (14) respectively.

Stemphol[8] (15) and antibiotic DB-2073[9] (16) are derivatives of 2,5-dialkylresorcinols whose structures need confirmation. This is now achieved by alkylating the diene (6) with *n*-butyl bromide in the presence of potassium amide followed by reaction with oct-2-yne-1-al (17) resulting in the aromatic aldehyde (18) which on decarbonylation with Wilkinson's catalyst followed by demethylation gave stemphol (15) in good yield. Similar alkylation of diene with hexyl bromide followed by cycloaddition with hex-2-yne-1-al (19) and subsequent transformation afforded the antibiotic DB-2073. This method has been extended to the synthesis of a number of alkyl resorcinols by alkylation of the diene (6) with appropriate alkyl halide

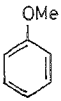

(1)

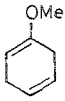

(2)

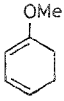

(3)

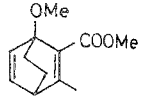

(4)

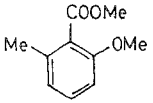

(5)

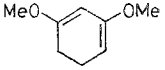

(6)

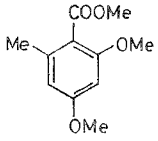

(7)

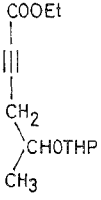

(8)

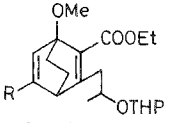

9 a. R=H
b. R=OMe

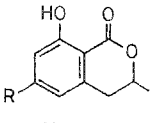

10 a. R=H
b R=OMe

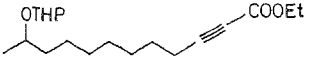

(11)

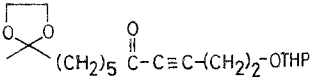

(12)

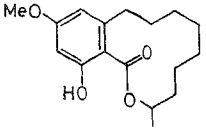

(13)

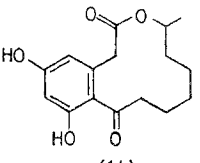

(14)

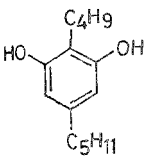

(15)

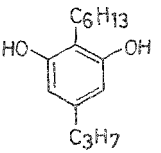

(16)

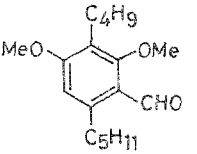

(18)

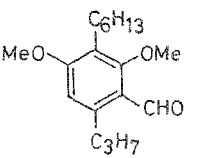

(20)

R–C≡C–CHO

(17) R = C_5H_{11}

(19) R = C_3H_7

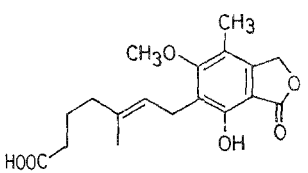

(21)

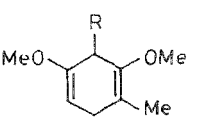

(22) R=H

(23) R=geranyl

followed by cycloaddition reaction with acetylenic aldehydes under Alder–Rickert reaction conditions.

Mycophenolic acid[10] (21) is a fungal metabolite, having gained considerable importance as an antitumour antibiotic. Its synthesis has been attempted by constructing the aromatic moiety from the diene (23) obtained by the alkylation of the diene (22) with geranyl bromide.

References

1. BIRCH, A.J. AND DONOVAN, F.W. *Aust. J. Chem.*, 1953, **6**, 360.

2. KANAKAM, C.C. — *Mechanism of metal-ammonia reduction and the synthetic utility of cyclohexadienes.* Ph.D. thesis, Indian Institute of Science, 1981.

3. BIRCH, A.J. AND SUBBA RAO, G.S.R. — *Adv. Org. Chem., Meth. Results*, 1972, **8**, 1-65.

4. GROVE, J.F. AND POPLE, M. — *J. Chem. Soc., Perk.I*, 1979, p. 2048.

5. SLATES, H.L., WEBER, S. AND WENDLER, N. — *Chimia*, 1967, **21**, 468.

6. ALDRIDGE, D.C., GALT, S., GILES, D. AND TURNER, W.B. — *J. Chem. Soc.*, 1971, p. 1623.

7. MUSGRAVE, O.C. — *J. Chem. Soc.*, 1956, p. 4301.

8. STODOLA, F.H., WEISLEDER, D. AND VESONDER, R.F. — *Phytochemistry*, 1973, **12**, 1797.

9. KANDA, N., ISHIZAKI, N., INOUE, N., OSHIMA, M., HANDA, A. AND KITAHARA, T. — *J. Antibiotics*, 1975, **28**, 935.

10. BIRCH, A.J. AND WRIGHT, J.J. — *Aust. J. Chem.*, 1969, **22**, 2635.

Thesis Abstract (Ph. D.)

Development of algorithms for optimum allocation of reactive powder in transmission and distribution systems by D. Thukaram.
Research supervisors: K. Parthasarathy and B. S. Ramakrishna Iyengar.
Department: Electrical Engineering.

1. Introduction

Present day power systems are complex and have grown very large. It is now more important than ever to design and operate power systems with highest degree of practicable efficiency, security and reliability. Active and reactive power optimization is becoming an increasingly important dispatching centre function in order to improve the quality of power supply and to judiciously operate the existing resources by minimizing the generation costs and system losses. While active power optimization is dominated by economic objective of minimizing generation costs, reactive power optimization concerns with re-distribution of reactive power to improve the system voltage profile and thereby minimize the active power losses. Further, reactive power optimization has grown in importance due to exploitation of

hydro and nuclear power generating sources at remote places and inclusion of long EHV AC as well as DC transmission networks in the system. Considerable work has been carried out in the area of active power optimization (economic dispatch) and work in the area of reactive power optimization has received attention only in recent times. This thesis concentrates around reactive power optimization in power systems. Systematic approaches to the coordinated distribution of reactive power in transmission and distribution systems have been developed and implemented on several practical power systems.

2. Scope of the present work

The problem of reactive power optimization in power systems is of two-fold *viz.*, a) planning of reactive power equipment in a system and, b) reactive power dispatch. Planning of reactive power in a system is directed at system conditions ranging from several months to several years in future. This involves the sizing and placing of additional reactive power support equipment in order to satisfy the system voltage limitations under both normal and contingency conditions. Reactive power dispatch can be defined as the control of generator excitation variables, transformer tap settings and adjustable VAR compensating devices to improve the system voltage profile and thereby to minimize the active power losses in the system. The associated analyses are performed minutes to hours prior to its implementation. At heavy/light load periods, voltage control is provided by controllable reactive sources. Some of the areas selected for development of algorithms for optimum allocation of reactive power in power systems are presented in the following sections.

3. Optimum reactive power dispatch

The major tool used for a reactive power dispatching strategy is an optimal power flow program. Since the introduction of optimal power flow method by Dommel and Tinney[1] many articles have appeared on this subject. In order to handle large scale problems, the idea of decomposition of optimal power flow problem into two, *viz.*, active power optimization and reactive power optimization is also used by many investigators[2]. Effective use of linear programming approximation to this non-linear problem is also reported in literature. Recently Mamandur and Chenoweth[3] presented a method for optimal control of reactive power flow employing linearized sensitivity relationships of power systems to establish both the objective function for minimizing the system losses and the system performance sensitivities relating the dependent and control variables. The approach adopted by the above authors has good potential for practical application of the algorithm. However, the algorithm needs further improvements for implementation to large power systems and real time applications. The application of optimal power flow program for reactive power dispatch and control in real time is presently in its infancy. This

requires the development of a security constrained optimal power flow, which computes in less than 5 minutes. Researchers are presently trying to solve this problem[4].

In this thesis an improved algorithm for reactive power optimization has been presented[5]. The approach involves an iterative scheme with successive solution of steady-state power flows and optimization of reactive power control variables using linear programming technique. The optimization problem is formulated by avoiding the inversion of large matrices. Fast de-coupled load-flow technique has been used for the successive power-flow solutions. Revised simplex technique *via* dual linear programming problem and also upperbound optimization techniques have been used for the solution of the optimization problem. The algorithm presented is efficient and less core demanding. The proposed algorithm has been successfully applied to large practical power systems and the results obtained for a few systems are presented.

HVDC transmission is now becoming an acceptable alternative to AC and is proving an economical solution not only for very long distance but also for underground and submarine transmission as well as a means of interconnecting systems of different frequency. Since the DC system alone does not generate any reactive power, a sequential approach for coordinated allocation of reactive power in AC/DC systems has been presented in this thesis.

The literature survey shows that very few articles discuss about the load characteristics, while the voltage profile in the system is forced to change by the application of reactive power optimization in a system. In case of interconnected power systems it is also necessary to consider the generation and tie-line control effects in the model. This thesis presents a method for optimum allocation of reactive power in large inter-connected power systems[6]. The model developed incorporates load and generation characteristics and also the effects of the tie-line controls. Results obtained on a practical system have been presented for different tie-line control strategies. The practical importance of the model developed has been demonstrated by comparing the results with those of conventional methods.

4. Optimum reactive power planning

Reactive power planning approaches involving optimization techniques, generally require an initial system condition which is a converged steady-state power flow solution. For some power systems it may not be possible to realize a converged power flow solution for a set of conditions. An initial starting point far from the optimum solution may lead to tremendous computational burden on the optimization problem. This thesis presents a method for estimation of reactive power requirements in the planning phase of a system. Considering the key nodes in the system as PV-load buses, a power flow method has been presented which helps in

getting a converged solution even for a severe contingency case. The proposed method has been tested by performing certain planning studies of a few Indian power systems. Results obtained on a typical systems are presented.

Power systems are in steady state only for a short duration. Frequent changes disturb the steady state so that the system is almost always in transition between steady-state conditions. Hence reactive power planning has to be based on both steady state and dynamic conditions. Following this trend, this thesis presents a comparative analyses of dynamic VAR planning in a power system having cyclic load, typical of a steel plant.

5. Reactive power compensation in distribution systems

The energy losses in distribution systems are generally quite appreciable constituting a major portion of the overall system losses. Installation of reactive power sources at suitable locations in distribution systems is usually suggested for dual purpose of achieving improved voltage profile and reduction in active power losses. This thesis presents algorithms for optimum size and location of reactive power requirements in complex distribution systems, typical of urban, with combination of radial as well as ring-main feeders and having different voltage levels. In addition, a novel method has been developed for finding optimum location of feeding point/reactive power compensation point in radial distribution systems[7]. In the analyses of radial distribution systems an important observation made is that the optimum location of the feed-point is more effective than the reactive power compensation both in terms of system performance and economy. Also, a reliable computationally-efficient method for power flow solution of radial distribution system is developed and illustrated.

6. Unbalanced reactive power compensation

Phase-wise unbalanced reactive power demand is caused in power systems due to large single phase loads and also due to large and fluctuating industrial loads such as electric arc furnaces, rolling mills, etc. Static VAR compensators (SVCs) are preferred over the traditional VAR compensators. The operation of thyristor-controlled compensators at various conduction angles can advantageously be used to meet the unbalanced reactive power demands in a system. However, such operation introduces harmonic currents into the AC system. In such cases it becomes necessary either to minimize harmonic generation internally or provide external harmonic filters. This thesis presents an algorithm[8] to evaluate an optimum combination of the phase-wise reactive power generations from SVC and balanced reactive power supply from the AC system based on the defined performance indices *viz.* Telephone Influence Factor (TIF), Total Harmonic Current Factor (IT), and Distortion Factor (D).

7. Conclusions

The developed algorithms have been successfully applied to practical power systems and the results obtained for various systems have been presented for illustration purposes. They are useful to both researchers and practising engineers.

References

1. DOMMEL, H. W. AND TINNEY, W. F. — Optimal power flow solutions, *IEEE Trans., PAS*, 1968, 87, 1866–1876.
2. CHAMOREL, P. A. AND GERMOND, A. J. — An efficient constrained power flow technique based on active-reactive decoupling and the use of linear programming, *IEEE Trans., PAS*, 1982, **101**, 158–166.
3. MAMANDUR, K. R. C. AND CHENOWETH, R. D. — Optimal control of reactive power flow for improvements in voltage profiles and for real power loss minimization, *IEEE Trans., PAS*, 1981, **100**, 3185–3194.
4. MILLER, T. J. E. — *Reactive power control in electric systems*, John Wiley & Sons, Inc., 1982.
5. THUKARAM, D., PARTHASARATHY, K. AND PRIOR, D. L. — Improved algorithm for optimum reactive power allocation, *Int. J. Elecl Power Energy Systems*, 1984, **6**, 72–74.
6. THUKARAM, D., PARTHASARATHY, K. AND RAMAKRISHNA IYENGAR, B. S. — Optimum reactive power control in an interconnected power system. Int Symp on Power Systems Engng, Wroclaw, Poland, Sept. 1985. pp. 283–288, Scientific papers of the Institute of Electric Power Engineering of the Technical University of Wroclaw, No. 65, Conf. No. 21, 1985.
7. THUKARAM, D., PARTHASARATHY, K., AND RAMAKRISHNA IYENGAR, B. S. — Optimum evaluation of reactive power requirements in power distribution systems, *Electric Mach. Power Systems* (USA), 1985, **10**(4), 261–272.
8. THUKARAM, D., PARTHASARATHY, K., AND RAMAKRISHNA IYENGAR, B. S. — Optimum control strategy of static VAR compensators for unbalanced reactive power demands, IEEE Conf. on Computers, Systems and Signal Processing, Bangalore, India, Dec. 1984, pp. 237–240.

Thesis Abstract (Ph.D.)

Sensitivity-based evolution design and evaluation of filter structures by K. Rajgopal.
Research supervisor: Late K. Ramakrishna.
Department: Electrical Engineering.

The design of high order filters poses many practical problems whether the implementation is in passive, active or in discrete domain. The passive component variation becomes important in the first two implementations while the non-ideal behaviour of the active devices[1], most often an operational amplifier (OA),

significantly influences the practical performance of RC-active filters. In discrete domain, it is the coefficient quantization which leads to quantization errors, product quantization noise, and finite wordlength effects. One common thread that links the non-ideal behaviour of filters in both analog and discrete domains is the sensitivity of a specific performance objective of the filter with respect to parameters like temperature, finite gain of the OA, finite wordlength in processing, and so on. This thesis predominantly emphasises the effectiveness of the sensitivity in the evolution, design and comparative evaluation of filter structures. The main objective of the investigations has been to evolve procedures leading to improved practical realisation of filters.

The thesis is in six chapters, the first chapter being an introduction to the work. The second chapter discusses the formulae and important properties relating to the first order sensitivity function[2]. Sensitivity invariants[3,4] linking several possible realisations of a function and bounds on sensitivity performance of lossless and RC-active networks are given.

The third chapter is devoted to the study of the converse problem[5] of the Blostein's[3] well-known multiparameter sensitivity invariance relation. The converse problem can be posed as follows. Let $F(w)$ be a rational function in w with real coefficients given by

$$F(w) = \frac{\sum_{j=0}^{n} a_j w^j}{\sum_{j=0}^{n} b_j w^j}$$

where w is a general independent complex variable and coefficients a_j and b_j are influenced by a set of real parameters X_i, $i = 1,2,\ldots,N$. The problem is to find functions of a_j and b_j of $(X_1,X_2,\ldots,X_N)$ that satisfy the multiparameter sensitivity criterion

$$\sum_{i=1}^{N} S[F(w;X_1,X_2,\ldots,X_N),X_i] = S[F(w;X_1,X_2,\ldots,X_N),w]$$

where $S[F(w;X_1,X_2,\ldots,X_N),X_i]$ and $S[F(w;X_1,X_2,\ldots,X_N),w]$ are first order sensitivity functions of F.

This relation is a generalised form of the original sensitivity invariance relationship in the analog domain due to Blostein[3], and is conceived as a basic criterion for evolving structures. One class of solution which satisfies the above relation is, when the coefficients a_j and b_j are weighted sums of all the products of the j different parameters chosen from the set $[X_i]$, of the form[5]

$$a_j = \sum_{J=1}^{{}^{N}C_j} a_{j,r} P_{jr}$$

$$b_j = \sum_{J=1}^{{}^{N}C_j} b_{j,r} P_{jr} \qquad j = 1,2,..,n$$

where P_{jr} is one of the ${}^{N}C_j$ possible products of j different parameters chosen from the set $(X_1, X_2, ..., X_N)$. $a_{j,r}$ and P_{jr} are real constants.

It is shown[6] that the above form of the solution to the converse problem encompasses all the possible realisations of a physically-realisable network function in the analog domain. Starting from this premise, new structures are shown to originate in analog and discrete domains, in addition to providing a better appreciation of known structures.

Chapter IV considers the worstcase sensitivity (WS) performance of several realisations of a transfer function $H(z)$ in discrete domain obtained from an analog transfer function $H_a(s)$ by using bilinear transformation, when sampling frequency w_s is varied. It is shown[7] that first order sensitivity functions of $H(z)$ with respect to the coefficients are transfer functions in z, with their coefficients again being nth order polynomials in C (mapping constant of the bilinear transformation). From the above relation it has been shown that the large sensitivities obtained in discrete filters, compared corresponding analog filters, is closely related to the sampling frequencies used. The influence of varying the sampling frequency w_s on the WS of $H(z)$ for different realisations has been analysed and shown to drop by nearly four orders, corresponding to a change in sampling frequency of less than two octaves. The corresponding influence on the minimum wordlength needed to realise the transfer function satisfying the specifications is illustrated.

In chapter V practical design aspects of high order filters with non-ideal components and devices are discussed. This chapter is a combination of three studies. A simple design procedure is given for the realisation of high order doubly-terminated LC ladder filters using a limited inventory of commercially available capacitor values. The procedure involves the principle of degenerating a high order ladder network into a smaller second order resonant circuits. The degenerate circuits along with their characteristic frequencies are used iteratively to obtain the values of elements of the overall network using only a set of standard capacitor values. This procedure is extendible to simulated RC-active ladder structures as well as to a large variety of realisations.

The non-ideal behaviour of the two-OA GIC realisations of the impedances due to finite gain A_0, gain bandwidth B, non-zero output resistance R_0 of OA and their higher order effects, signal handling capability (SHC) and noise performance have been consolidated. The design of two-OA GIC for LPF and BPF has been consolidated essentially based on the RC-optimisation of the simulated impedance

satisfying on one hand the constraints on the element values due to SHC of the OA, and minimising the output noise of the GIC, while also having a satisfactory deviation and quality factor Q performances over a wide range of frequencies. The design procedure involves choice of some important parameters based on signal levels across the impedance of the filter, sensitivity behaviour of the filter structure and finally the non-ideal parameters of the OA.

It has been pointed[8] out that the design philosophy of RC-active highpass filters is entirely different compared to LPF and BPF, since the passband ideally extends to infinity. The practical requirement of a reasonable passband behaviour in HPF, at least up to 10 times the corner frequency, is comparatively difficult to achieve due to deteriorating performance of the practical OAs. Improvement in the high frequency performance of highpass filters has been achieved[8,9] essentially by adapting the design of two-OA GIC. The GIC is RC-optimised at a suitable frequency ω_D higher than the corner frequency ω_c of the highpass filter so as to obtain a satisfactory performance of deviation and Q over a wider range of frequencies. The upper limit on ω_D has been suggested, based on the design experience of LPF and BPF, as B/50 without introducing excessive nonideal effects on the GIC at high frequencies. Further, if a passband performance is to be obtained at least up to $\omega_H = 10\omega_c$ (ω_H is the highest frequency up to which the passband performance is desired) in a highpass filter, then the minimum limit on the gain bandwidth B desired of the OA, chosen for the realisation of a high quality GIC, is suggested as $B > 25\omega_H$. The low sensitivity at higher frequencies of HPF[9] realised using ladder structure forms a part of the design procedure. Two HPF examples with corner frequencies at 10 kHz and 30 kHz have been designed and experimentally evaluated using amplifiers with different gain bandwidths B, to show the effectiveness of the design procedure. The experimental results clearly show that a passband performance for frequencies $\omega_H \geq 10\omega_c$ is obtained nearly satisfying the stringent specifications of 0.1 dB variation in the passband of a 7th order Cauer–Chebyshev HP filters. The design procedures also take into consideration the constraints on the maximum and minimum values of the RC elements dictated by the ease of manufacturing processes involved in microcircuit technology.

Chapter VI suggests scope for further work particularly in the area of evolving filter structures based on multiparameter sensitivity criterion and its generalisation to multivariable systems.

References

1. Ramakrishna, K., Soundararajan, K. and Aatre, V. K. — Effects of amplifier imperfections on active networks, *IEEE Trans. Circuits Systems*, 1979, **CAS-26**(11), 922–930.

2. Bruton, L. T. — *RC-active circuits: Theory and design*, Prentice-Hall Inc., Englewood Cliffs, N.J., 1980.

3. BLOSTEIN, M. L.	Sensitivity analysis of parasitic effects in resistance terminated IC two-pots, *IEEE Trans. Circuit Theory*, 1967, **CT-14**(2), 21–25.
4. VENKATESHA MURTHY, K. V.	Sensitivity considerations in network synthesis, Master's Thesis, Department of Electrical Engineering, Indian Institute of Technology, Bombay, 1967.
5. RAMAKRISHNA, K.	Filter structures originating from a multiparameter sensitivity criterion, *IEEE Int. Symp. Circuits Systems*, Newport Beach, USA, May2–4, 1983, pp. 278–281.
6. RAMAKRISHNA, K. AND RAJGOPAL, K.	A unified approach to structures in s-domain originating from a multi-parameter sensitivity criterion, *IEEE Int. Conf. Computers, Systems Signal Processing*, Bangalore, India, Dec. 10–12, 1984.
7. RAMAKRISHNA, K. AND RAJGOPAL, K.	On the effects of varying sampling rate on the performance of digital filters, *IEEE Int. Symp. Circuits Systems*, Montreal, Canada, May 7–10, 1984.
8. RAMAKRISHNA, K. AND RAJGOPAL, K.	On the design of RC-active highpass filters, *Proc. 25th Midwest Symp. Circuits Systems*, Houghton, Michigan, Aug., 1982.
9. RAMAKRISHNA, K. AND RAJGOPAL, K.	On the design of RC-active highpass filters using 2-OA GIC, *Can. Electl Engng J.*, 1985, **10**, 69–75.

Thesis Abstract (M.Sc. Engng)

Prediction of compressibility of natural soils by Bindumadhava.
Research supervisors: T. S. Nagaraj and B. R. Srinivasa Murthy.
Department: Civil Engineering.

1. Introduction

Inherent nature and diversity of geological processes involved in soil formation are responsible for the complexity of the soil system. The property characterization of such a complex system involves elaborate time-consuming laboratory testing. It has been the fervent desire of geotechnical engineers to evolve simple testing methods both in the laboratory and the field such that with minimum input of parameters the soil behaviour can be predicted.

Attempts have been made in this Institute recently[1–5] to generalize and rationally predict the compressibility behaviour of fine-grained soils. In this investigation attempt has been made to extend the above generalization to saturated uncemented natural soils, which contain coarser particles as solid constituents.

2. Re-examination of the micro-model

Nagaraj and Srinivasa Murthy[2] have shown that the unique half-space distance, d *vs* net osmotic repulsive pressure (R–A) relationship[6] derived from the Gouy-

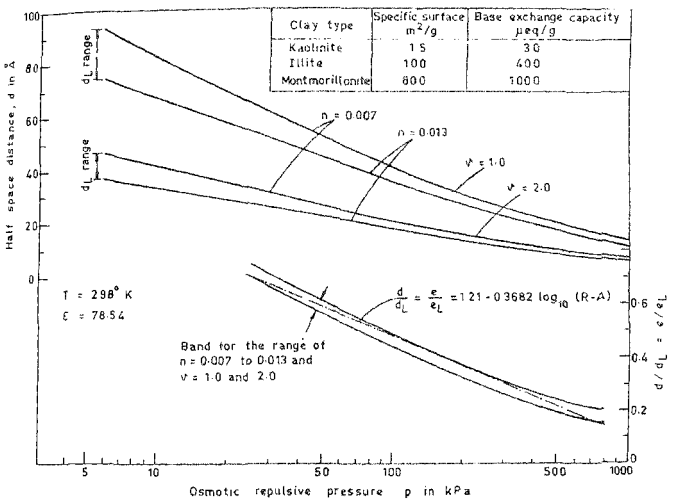

FIG. 1. Analytical $d - \log p$ and $(e/e_L) - \log_{10} p$ relationships.

Chapman diffuse double layer theory provides the basis to generalize the compressibility behaviour of normally consolidated saturated uncemented fine grained soils, for a given physico-chemical environment. To ensure generality of the compressibility equation, this micro-model has been re-examined by considering the variation in the values of the physico-chemical environmental factors (fig. 1).

Using the Gouy-Chapman diffuse double-layer theory and the method of computation proposed by Sridharan and Jayadeva[6], the d *vs* (R–A) relationships have been computed for three clays for defined combinations of bulk solution concentration, n and valency of cation, v. Figure 1 indicates the special spread of d *vs* (R–A) plots for various combinations. From the void ratio, e, specific surface, S and the half space distance, d relationship, it can be shown that

$$d/d_L = e/e_L$$

where d_L and e_L are half-space distance between clay particles and void ratio at liquid limit respectively. Thus the d *vs* (R–A) relationships of fig. 1 can be transformed into (e/e_L) *vs* (R–A) relationship by normalising with their respective d_L values. It is interesting to note that the d *vs* log (R–A) plots which are distinctly

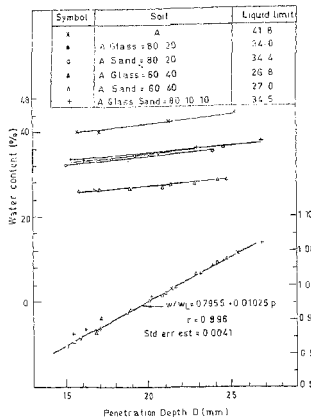

FIG. 2. Experimental flow curves and $w/w_L - D$ relationship.

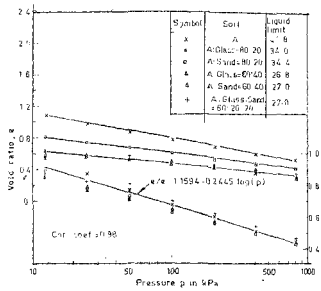

FIG. 3. Experimental $e - \log_{10} p$ and $(e/e_L) - \log_{10} p$ plots.

different for different combinations of the physico-chemical environmental factors, collapse into a very narrow band in the (e/e_L) *vs* log (R–A) plot. This implies that (e/e_L) *vs* (R–A) relationship is more general and fundamental, with e_L accounting for physico-chemical environmental factors in addition to the specific surface of the soil.

Modified liquid limit

The effect of coarse fractions in soils on their liquid limit has been experimentally studied. This has been attempted by generating flow curves of three natural soils (having liquid limit values of 42, 68 and 92 per cent) mixed with different percentages of coarse particles. The coarse particles used are crushed sand and smooth spherical uniform glass particles, which have different surface frictional characteristics, shape and size. It has been shown that the coarse particles reduce the liquid limit in proportion to the percentage of coarse particles irrespective of their type, size and shape. These flow curves can be normalised with their (respective) liquid limits, to result in a unique line (fig. 2). The behaviour has been explained in terms of the floating matrix concept. The quantification of this concept has been made in terms of the modified liquid limit, for the per cent and size of the coarse particles used in this investigation.

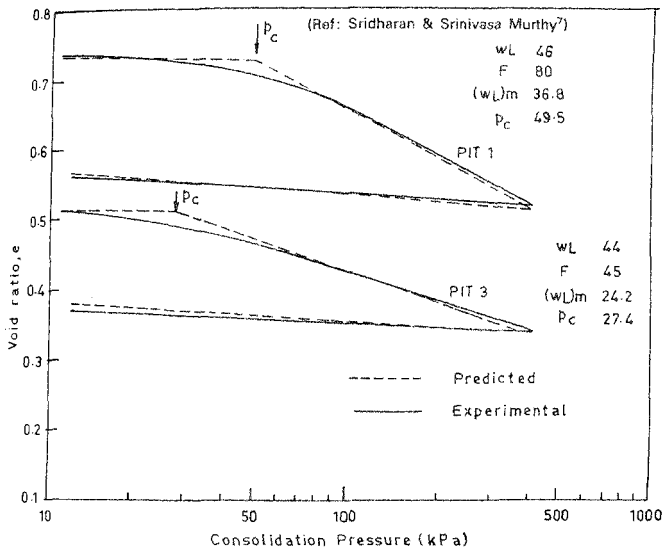

FIG. 4. Prediction of compressibility behaviour.

Compressibility behaviour

The effect of coarse particles on compressibility has been studied in relation to the laboratory-generated $e - \log p$ curves. It is shown that the $e - \log p$ curves of soils having coarse material as admixtures can be normalized using their respective modified liquid limit values (fig. 3). Further, using the modified liquid limit values, the generalized models proposed by earlier investigators can be used effectively to predict the compressibility behaviour of natural soils having coarser particles also (fig. 4).

Simplified method of determining the liquid limit

In the above predictive methods, if liquid limit is known, the compressibility behaviour can be predicted, perhaps within a very short period. But in normal practice the liquid limit determination itself takes more than 24 hours. There exists

Table I

Reproducibility of experimental liquid limit results by bulk density method

Soil	Wt of soil filled (g)	γ_b (g/cc)	Water content %	Specific gravity G	S_r (%)	Computed water content	Depth of penetration in mm.	% Error $(\vartheta) = \frac{(4)-(7)}{(4)} \times 100$
A	167·26	1·761	43·26	2·70	97·58	43·68	25·4	0·97
	167·36	1·762			97·69	43·57	25·6	0·72
	168·26	1·771	42·22	2·70	97·59	42·61	21·5	0·92
	168·46	1·773			97·81	42·40	21·5	0·43
	169·71	1·786	41·08	2·70	97·97	41·12	15·9	0·10
	169·93	1·789			98·20	40·90	15·3	0·44
B	147·41	1·552	73·72	2·70	98·41	72·91	27·9	1·10
	147·73	1·555			98·72	72·27	27·6	1·97
	148·62	1·564	71·79	2·70	98·65	70·53	24·9	1·76
	148·79	1·566			98·82	70·20	24·6	2·21
	151·48	1·595			98·34	65·29	16·9	0·90
	151·52	1·595	65·88	2·70	98·38	65·22	16·6	1·00
C	138·59	1·459	96·80	2·70	98·9	94·08	24·0	2·81
	138·71	1·460			99·0	93·74	23·8	3·16
	139·20	1·465	92·93	2·70	98·2	92·36	20·4	0·61
	139·25	1·466			98·3	92·22	20·8	0·76
	142·48	1·500	85·09	2·70	98·5	83·81	14·5	1·50
	142·32	1·498			98·4	84·20	13·9	1·05

Volume of the cup = 95·0 c.c.

an interrelationship between the water content, w and the bulk density, γ_b for a known degree of saturation, S_r in the form,

$$\gamma_b = \frac{G(1+\omega)}{1+\frac{G\omega}{Sr}}\gamma_\omega$$

where, G is specific gravity of soil particles and γ_w is unit weight of water

In the above equation for known value of the degree of saturation, specific gravity and bulk density, water content can be determined instantaneously. In liquid limit determination using cone penetrometer the bulk density of the soil can be determined by measuring the weight and volume of the cup filled with soil. From an extensive experimental data, it has been found that the degree of saturation in such tests is about 98%. This principle has been used to determine water content instantaneously in the liquid limit determination. Table I indicates the reproducibility of test results by this simplified method of computing liquid limit. The error in

the liquid limit computed by the proposed method is within the limits of accuracy at engineering level.

3. Conclusions

Based on the basic considerations, experimental results and discussions presented in this investigation, the following specific conclusions have been drawn.

1. The (e/e_L) *vs* (R–A) relationship is more general and fundamental than the d *vs* (R–A) relationship.
2. The liquid limit of soil reduces linearly with addition of coarse particles. The size, shape and surface characteristics of coarse particles do not influence the type of interactions at liquid limit level, other than the linear reduction in specific surface. The reduced liquid limit is defined as the 'modified liquid limit'.
3. The presence of coarse particles will only dilute the compressibility behaviour of the soil in proportion to the corresponding reduction in liquid limit of soil. The variation in the surface characteristics, shape and size of coarse particles present does not influence the compressibility behaviour of the fine grained soil.
4. The modified liquid limit can be effectively used to predict the compressibility behaviour of saturated uncemented fine-grained soils, having coarser particles.
5. A simplified method of determining the water content with the cone penetrometer cup and using the basic interrelationship between the water content and bulk density has been brought out. This can be gainfully used for instantaneous determination of liquid limit of the fine-grained soils.

References

1. Srinivasa Murthy, B.R. — Prediction of volume change behaviour of soils, Ph.D Thesis, Indian Institute of Science, 1983.
2. Nagaraj, T.S. and Srinivasa Murthy, B.R. — Rationalization of Skempton's compressibility equation, *Geotechnique*, 1983, **33**(4), 433–443.
3. Nagaraj, T.S. — Prediction of soil behaviour, *Proc. Symp. recent developments in laboratory and field tests and analysis of geotechnical problems*, AIT, Bangkok, 1983.
4. Nagaraj, T.S. and Srinivasa Murthy, B.R. — Prediction of pre-consolidation pressure and recompression index, *Geotech. Testing, J. ASTM*, 1985, **8**(4), 199–203.
5. Nagaraj, T.S. and Srinivasa Murthy, B.R. — Prediction of compressibility of over consolidated soils, *J. ASCE, Geotech. Div.*, 1986, **112**(GT4), 484–488.
6. Sridharan, A. and Jayadeva, M.S. — Double layer theory and compressibility of clays, *Geotechnique*, 1982, **32**(2), 133–144.
7. Sridharan, A. and Srinivasa Murthy, B.R. — Consultancy Report No. CP. 33/122/85–156, Civil Engineering Department, Indian Institute of Science, 1985.

Thesis Abstract (M.Sc. Engng)

Dielectric-coated corner reflector by Nemichandramma.
Research Supervisor: A. Kumar.
Department: Electrical Communication Engineering.

Introduction

The electromagnetic field of an antenna may be obtained by solving Maxwell's field equations rigorously subject to the appropriate boundary conditions which must include not only the boundary conditions applicable at the exciting source but also those applicable at infinity. Because of these complications, exact solution can not be obtained except in a few simple cases. Therefore, various approximate methods are employed to calculate the radiation field of an antenna. Ray theory is one such technique which yields, particularly at high frequencies, practically acceptable results. It is an extension of the geometrical optics to the microwave region of electromagnetic spectrum[1].

Infinite conducting plane

The radiation pattern of an isotropic antenna in the presence of an infinite conducting plane is derived by employing the ray theory technique.

Consider an isotropic source placed at the origin, S, of a spherical polar co-ordinate system, a distance, d, above a perfectly conducting infinite plane as shown in fig. 1. The effect of the plane on the radiation pattern of the source at S, may be taken into account by replacing the conducting plane by an isotropic source, located at D, of the same magnitude as the source at S, but 180° out-of-phase with it. The total field at a far-off point, $P(r, \theta, \varnothing)$, is given by,

$$|E| = \sin(\beta d \cos\theta) \tag{1}$$

where $\beta = 2\pi/\lambda$.

Dielectric-coated infinite conducting plane

Consider the antenna system discussed above but with the difference that the infinite conducting plane has on it a uniform coating (of thickness t) of a lossless dielectric (dielectric constant ε_r) as shown in fig. 2. Employing ray theory, the analysis shows that the effect of the dielectric-coated infinite conducting plane may be taken into account by a linear array of equally spaced isotropic sources having a constant progressive phase shift, and located on the surface of the dielectric, coating, as shown in fig. 2.

The phase difference between any two consecutive rays is

$$\psi = 2\beta t \sqrt{\varepsilon_r - \sin^2\theta}. \tag{2}$$

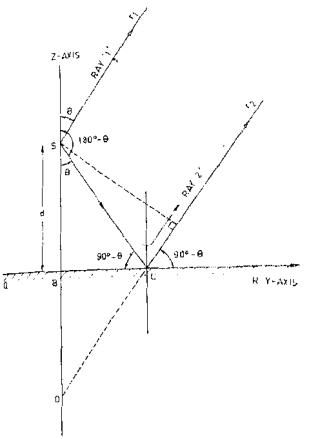

FIG. 1. An isotropic source placed above a perfectly conducting infinite plane.

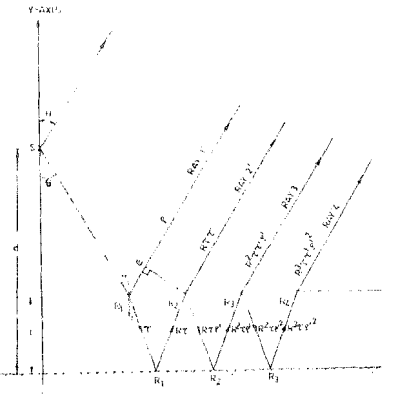

FIG. 2. An isotropic source above an infinite conducting plane having a uniform dielectric coating.

The amplitude of different rays are as labeled in fig. 2. The field at a distant point, P, is the vectorial sum of all these rays and the direct ray. The vectorial sum of these rays is given by

$$E_1 = \rho + R\ \tau\tau' \exp(-j\psi)\left[\frac{1}{1 - R\ \rho' \exp(-j\psi)}\right], \tag{3}$$

$$R = -1$$

where

ρ = reflection co-efficient in medium 1.

τ = transmission co-efficient in medium 1,
ρ' = reflection co-efficient in medium 2,
τ' = transmission co-efficient in medium 2.

Therefore, the total field at the distant point including the contribution of the direct ray is

$$E = 1 + \exp(-j\psi_{11})\,[E_1] \tag{4}$$

where ψ_{11} is the phase difference due to the path difference SF between the direct ray and ray '1'.

For the special case wherein the source is on the dielectric itself,

$$d = t \text{ , and } \psi_{11} = 2\beta(d - t)\cos\theta = 0.$$

Therefore, the above equation reduces to

$$|E| = \frac{2(1+\rho)\sin\psi/2}{\sqrt{+2\rho'\cos\psi+\rho'^2}}. \tag{5}$$

Taking an x-oriented horizontal Hertzian dipole antenna located on a dielectric-coated conducting plane, the above equation gives the radiation pattern in the YZ-plane.

The radiation patterns for $\varepsilon_r = 2.56$ (Teflon fibre glass) and $\varepsilon_r = 6.00$ (Beryllium oxide) have been computed using the above equation.

Results are in good agreement with those given by Shastri[2].

Corner reflector antenna[3]

Kraus[3] has analysed the corner reflector antenna system by employing the method of images. Moullin[4] has obtained an expression for the far-field of the corner reflector antenna system as an infinite series. The problem of the corner reflector antenna may also be tackled using ray theory.

The effect of the corner reflector on the radiation pattern of the source at S, may be taken into account by replacing the corner reflector by N isotropic sources, where N is the number of images formed by the corner reflector (fig. 3). Adopting the ray theory approach the total field at the far-off point, P, is given by

$$E = \frac{\exp(-j\beta r)}{r}\left[\sum_{n=0}^{N}\exp(j\psi_n)\right] \tag{6}$$

where $\psi_n = \beta(r - r_n) + \alpha_n$ and α_n is the phase angle by which the image at S_n leads the source at S.

For the case of a 90° corner reflector equation 6 simplifies to

$$E(\theta) = 2[\cos\{\beta R\cos(\psi/2-\theta)\} - \cos\{\beta R\cos(3\psi/2-\theta\}].$$

For the case of a 60° corner reflector equation 6 simplifies to

$$E(\theta) = j2[\sin\{\beta R\cos(\psi/2-\theta)\} - \sin\{\beta R\cos(3\psi/2-\theta)\} + \sin\{\beta R\cos(5\psi/2-\theta)\}].$$

Of particular interest is the value of the field, $E(\psi/2)$, along the direction $\theta = \psi/2$.

For the various radial location R of the driven element, on the bisecting plane of the apex angle, the field is computed using the following equations

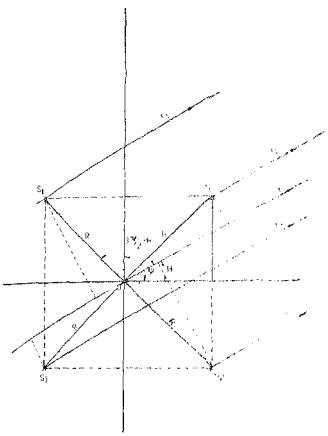

FIG. 3. Isotropic source in a 90°-corner reflector.

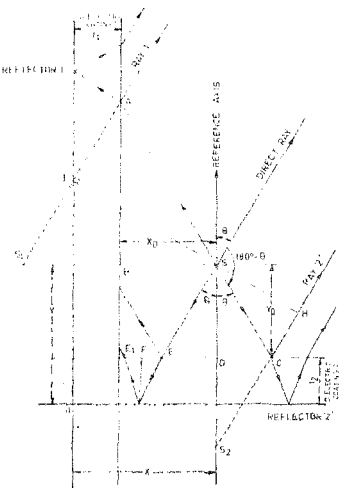

FIG. 4. Dielectric-coated corner reflector.

$$E(\psi/2) = [\cos(\beta r) - \cos(\beta r \cos \psi)]$$

for the 90° corner reflector,

$$E(\psi/2) = j2[\sin(\beta R) - \sin(\beta R \cos \psi) + \sin\{\beta R \cos(2\psi)\}]$$

for the 60° corner reflector.

Results are in good agreement with those of Moullin's[4].

Dielectric-coated corner reflector antennas

Consider an isotropic source place at the origin, S, in a 90° corner reflector coated with a lossless dielectric (dielectric constant ε_r). This corner reflector can not be replaced just by three images as in the case of 90° corner reflector without the dielectric coating. The dielectric coating over a reflecting surface results in multiple reflections of any ray that is incident on the dielectric coating. The results of summing up these multiple reflected rays is to produce an equavalent reflected ray whose amplitude is M times that of the incident ray, where M is given by

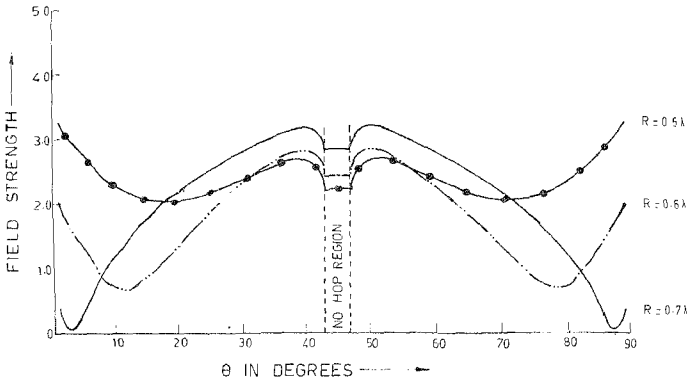

FIG. 5. Radiation pattern of an isotropic source placed in a dielectric-coated corner reflector.

$$M = \rho - \frac{\tau\tau' \exp(-j\psi)}{1+\rho' \exp(-j\psi)} \quad .$$

Analysis shows that the radiation from the source in any direction consists of the following components.

1. Direct ray from the source in the direction θ.
2. Ray leaving from the source along the direction $(180° - \theta)$, getting reflected from reflector '2'.
3. Ray leaving from the source along the direction $(360° - \theta)$, getting reflected from reflector '1'.
4. Ray leaving from the source at $(180° + \theta)$, getting reflected from both reflectors.

To find the net radiation field at a far-off point due to the antenna system, above mentioned rays will have to be added in proper phase and amplitude.

Let the multiple reflection factor for the reflectors '1' and '2' be M_1 and M_2 respectively. The phase difference, ψ_{11}, ψ_{11}, between the direct ray and ray '1' and the phase difference ψ_{22}, between the direct ray and ray '2' is given by

$$\psi_{11} = \beta \times S_1 I \qquad \psi_{22} = \beta \times S_2 H.$$

For the ray directed along $(180° + \theta)$, depending on the geometry (fig. 4) two cases of reflection arise.

Case I: The distance, AB, is more than the distance, SD. In this case, if there are n reflections (n hops) at the dielectric '2' –air interface, before the ray enters the dielectric coating '1', there will be $(n+1)$ emergent rays.

Case II: The distance, AB, is less than the distance, SD. In this case it is noted that, if there are n reflections at the dielectric '1'–air interface, before the ray enters the dielectric coating '1', there will be $(n+1)$ emergent rays.

The net radiation field at a far-off point simplfies to

$$E = 1 + M_1 \exp(j\psi_{11}) + M_2 \exp(j\psi_{22}) + M_1 \rho \exp(j\beta\rho_0) \text{ for } n = 0$$

$$E = 1 + M_1 \exp(j\psi_{11}) + M_2 \exp(j\psi_{22}) + M_1 \rho \exp(j\beta\rho_0) + M_1 \sum_{k=1}^{n} R^k \tau\tau' \rho'^{k-1} \exp(j\beta(\rho_0 + 2m_1 k)) \text{ for } n \neq 0 \text{ for Case I}$$

$$E = 1 + M_1 \exp(j\psi_{11}) + M_2 \exp(j\psi_{22}) + M_2 \rho^{11} \exp(j\beta\rho_0) \text{ for } n = 0$$

$$E = 1 + M_1 \exp(j\psi_{11}) + M_2 \exp(j\psi_{22}) + M_2 \rho^{11} \exp(j\beta\rho_0) + M_2 \sum_{k=1}^{n} R^k \tau\tau' \rho''^{k-1} \exp(j\beta(\rho_0 + 2m_2 k)) \text{ for } n \neq 0 \text{ for Case II}$$

where P_k is the path difference of the ray 'α_k' with respect to the direct ray

$$m_1 = 2t_2 \cos^2\theta/\sqrt{\varepsilon_r}\cos(r) \quad m_2 = 2t_1 \cos^2(90-\theta)/\sqrt{\varepsilon_r}\cos(r^1).$$

For various radial locations of the driven element, on the bisecting plane of the apex angle, the radiation pattern in the plane normal to the two reflectors is computed using the above expression (fig. 5). It may be observed from the graphs that the radiation pattern has side lobes. The number of side lobes increases as the radial distance of the driven element on the bisecting plane of the apex angle, increases. The direction of the major lobe depends on the thickness and the relative permittivity of the dielectric coating, and the radial location of the driven element.

As the thickness of the dielectric coating decreases, the minima of the major lobe slightly pull down and there is a slight decrease in the side lobe level.

It is to be noted that there is 'no hop' region near the apex angle bisector. This results in small constriction of the radiation pattern near the bisector angle, 45°.

Concluding remarks

An advantage of dielectric coating configuration is that the dielectric layer over the reflecting planes acts as a protective layer. For the case of plane reflector, it is seen that by coating the reflector with suitable dielectric, there is little change in the

radiation pattern, as long as the thickness of the coating is comparatively small. For the case of corner reflector, a coating of dielectric results in a pattern which is complicated as compared to the corner reflector without the dielectric coating. The coating results in a slightly narrower major lobe for certain radial locations of the driven element. The radiation pattern has many side lobes. In cases where the existence of the side lobes can be tolerated, it is advantageous to coat the reflectors with a dielectric.

References

1. DESCHAMPS — Ray technique in electro-magnetism, *Proc. IEEE*, 1972, P, 1022.

2. SHASTRI, S. V. K. — *Conformal antennas*, Ph.D. Thesis, Indian Institute of Science, 1978.

3. KRAUS, J. D. — The corner reflector antenna. *Proc. IRE*, 1940, 28, 513.

4. MOULLIN, E. B. — *Radio aerials*, Clarendon Press, Oxford, 1949.